American Mineralogist, Volume 88, pages 1312–1317, 2003

Compressional and shear wave velocities of ringwoodite γ-Mg_2SiO_4 to 12 GPa

BAOSHENG LI*

Mineral Physics Institute, State University of New York at Stony Brook, Stony Brook, New York 11794-2100, U.S.A.

ABSTRACT

Compressional and shear wave velocities of ringwoodite (γ-Mg_2SiO_4) were measured on a polycrystalline specimen to 12 GPa at room temperature using ultrasonic interferometry techniques. Velocity measurements at ambient conditions yielded V_p = 9.86(3) and V_s = 5.78(2) km/s. Finite strain analysis of the high pressure velocity data yields K = 185(2) GPa, G = 120(1) GPa, K' = 4.5(2), and G' = 1.5(1) for the elastic moduli and their pressure derivatives, respectively. The velocities and elastic moduli at ambient conditions are indistinguishable from aggregate properties of polycrystalline ringwoodite calculated using single crystal elastic constants (C_{ij}). Comparison of the current results on pressure derivatives of bulk and shear moduli with previous acoustic data on iron free ringwoodite to 3 GPa and iron bearing sample to 16 GPa indicated that the discrepancy can be explained by the pressure range of the experiments rather than iron content. Current results suggest that ringwoodite and wadsleyite posses very similar pressure dependence in elastic properties to the transition zone depth. In a pyrolite mantle with 1400 °C adiabatic foot temperature, the wadsleyite to ringwoodite phase transition is characterized as a seismic reflector spreading about 20 km in width with a density jump of 2.1% and impedance jumps of 2.4% and 3.1% for P and S waves near 520 km depth, which is consistent with seismic observations in long period data.

INTRODUCTION

Ringwoodite is a high-pressure polymorph of olivine forming at a depth of approximately 520 km in the transition zone of the mantle. In a homogeneous pyrolitic mantle, the physical property change associated with phase transitions from olivine to wadsleyite and wadsleyite to ringwoodite have long been considered responsible for the seismic discontinuities at 410 and 520 km depths (e.g., Ringwood 1975; Katsura and Ito 1989; Bina and Wood 1987; Morishima et al. 1994 and references therein). Unlike the 410 km seismic discontinuity which has been observed worldwide in various studies, universal existence of the 520 km discontinuity is still controversial (e.g., Shearer 1991, 1996; Bock 1994; Benz and Vidale 1993; Flanagan and Shearer 1998; Ryberg et al. 1997). Long-period seismic studies (e.g., Shearer 1990, 1991; Revenaugh and Jordan 1991; Flanagan and Shearer 1998) report a diffuse impedance jump (~3%), but evidence for a 520 km discontinuity in short-period and precursor studies (e.g., Cummins et al. 1992; Benz and Vitale 1993) is less convincing. Although questions about the possibility of the 520 km discontinuity being an artifact in the processing of the long period data of Shearer (1990) were raised by Bock (1994), a later study by Shearer (1996) confirmed the existence of the discontinuity. The existence of 520 km global discontinuity (Shearer 1990, 1996) has also been challenged by the fact that it can be observed only in certain regions but not beneath continental shield (e.g., Ryberg et al. 1997; Gu et al. 1998). In a recent study using precursors to the SS phase, Deuss and Woodhouse (2001) observed splitting of the 520 km discontinuity, suggesting that compositional heterogeneity is responsible for the regional occurrence of single or double discontinuities around this depth.

Laboratory measurements of the elastic properties of wadsleyite and ringwoodite at high pressure and temperature provide insight into Earth's seismic features since a phase transition occurs at approximately 520 km depth. In the last few years, technical developments have enabled acoustic wave velocity measurements to transition zone pressures using ultrasonic and Brillouin scattering techniques. Application of these techniques to wadsleyite provided valuable data for shear properties which were not available from *P-V-T* EOS studies (e.g., Li et al. 1996b; Zha et al. 1998). Simultaneous ultrasonic velocity and X-ray diffraction measurements at high pressure and high temperature have also been reported for wadsleyite to 7 GPa and 873 K, yielding direct determination of bulk and shear moduli at pressure and temperature (Li et al. 1998a, 2001). For ringwoodite (γ-Mg_2SiO_4), Rigden et al. (1991) reported ultrasonic measurements to 3 GPa using a polycrystalline sample. Recently, elastic properties of an iron-bearing ringwoodite with composition γ-$(Mg_{.91}Fe_{.09})_2SiO_4$ have been measured to 16 GPa using Brillouin scattering (Sinogeikin et al. 2001). However, the pressure derivatives of bulk and shear moduli from these two studies differ by as much as ~20%. The reasons for these differences have been discussed in terms of the effect of iron and the pressure ranges of the different experiments and are further explained in our report.

In this study, velocity data for polycrystalline ringwoodite (γ-Mg_2SiO_4) to 12 GPa at room temperature are presented. The results are compared with previous measurements on iron-free and iron-bearing ringwoodite. Using previous data on wadsleyite, the physical property change across the phase transition from wadsleyite to ringwoodite and their implications for the 520 km discontinuity will be discussed.

* E-mail: bli@notes.cc.sunysb.edu

0003-004X/03/0809–1312$05.00

EXPERIMENTAL TECHNIQUES

The polycrystalline specimen was hot-pressed at about 20 GPa and 1200 °C for one hour in a 2000 ton Uniaxial Split Sphere Apparatus (USSA-2000) in the Stony Brook High Pressure Lab. Olivine (α-Mg_2SiO_4) powder was used as starting material. The product was examined by X-ray diffraction and full transformation to pure cubic ringwoodite was confirmed. A bulk density of 3.515(8) g/cm^3 was obtained using the immersion technique. The bulk density is within 99% of the X-ray density (3.559 g/cm^3, Weidner et al. 1984). The length of the sample after final polishing was 1.535(1) mm and the diameter was ~2.5 mm. Bench top velocity measurements were performed using glass buffer rods with 40 MHz $LiNbO_3$ transducers (36° Y-cut for compressional wave and 41° X-cut for shear wave), yielding V_p = 9.86(3) and V_s = 5.78(2) km/s, respectively. These values are in excellent agreement with previous single crystal results of V_p = 9.85–9.86 and V_s = 5.78–5.82 km/s using Brillouin scattering techniques (Weidner et al. 1984; Jackson et al. 2000).

Compressional and shear wave velocities to 12 GPa at room temperature were measured with a 1000 ton Uniaxial-Split Cylinder Apparatus (USCA-1000). High pressure is generated in two stages. The first stage pressurization is provided by uniaxial loading of the guide blocks, and the second stage consists of eight tungsten carbide (WC) cubes with triangular truncations on the corner of each cube. The assembled WC cubes create an octahedral space for hosting the pressure medium (e.g., Liebermann and Wang 1992). Ultrasonic measurements were implemented by mounting a piezoelectric transducer on an outside corner of one WC cube while its opposite corner is in contact with the sample, which is enclosed in pressure medium and surrounded by lead in a stainless sleeve (see Fig. 1b of Li et al. 1996a). To enhance the mechanical coupling between the WC cube and the sample for optimum acoustic wave propagation, a gold foil (2 μm thickness) was inserted at the WC cube/sample interface. Sample pressure was determined by monitoring the resistance change associated with phase transformations of the pressure markers (Bi and/or ZnTe). The pressure markers were placed in a teflon disk immediately adjacent to the sample to minimize the error in the estimation of sample pressure. Fitting the recorded ram loads to the pressures where the phase transformations occur (Bi, 2.55 and 7.7 GPa; ZnTe, 9.6 and 12 GPa) provides a pressure scale for each high pressure experiment. Two experiments were conducted for P-wave measurements, one with Bi only and the other using both Bi and ZnTe as pressure standards, up to 9.6 GPa and 12.1 GPa, respectively. S-wave velocity was measured with both Bi and ZnTe as pressure standards to 12.3 GPa.

To minimize the deviatoric stress applied to the sample during compression, the sample and the teflon disk were surrounded by lead and placed inside a steel sleeve. As examined at the end of the high pressure experiments, the sample exhibited no shortening or permanent deformation. Non-hydrostaticity and its effect on the measurements was not considered in this study, but it is believed to be small based on the dislocation density of a single crystal of olivine (Li et al. 1998b). It is likely that the major source of error is the experimental uncertainties in pressure as illustrated in Figure 2 of Li et al. (1998b).

Travel time was measured using the phase comparison method of ultrasonic interferometry and an acoustic interferometer from ANUTECH (e.g., Niesler and Jackson 1989). Details of this method have been described elsewhere (Niesler and Jackson 1989; Rigden et al. 1991; Li et al. 1996a). Briefly, when a gated RF pulse travels through the sample and is reflected back to the receiver, there is a phase delay between the front end reflection and the back end reflection due to additional round trip travel inside the sample. When the frequency of the RF input varies, the two reflections experience in-phase and out-of-phase delay, i.e., $\omega\Delta t = n\pi$, where Δt is the round trip travel time inside the sample. This results in a series of minima and maxima in the summation of the two reflections. The apparent travel time (Δt) is therefore obtained from the frequency (f) where these extrema occur, $\Delta t = n/2f$, where n is the number of the wavelength in the round trip distance of the sample length. In this study, the P-wave travel time was obtained in the frequency range 40–60 MHz, and S wave in the range 30–50 MHz. The perturbation of the gold foil to the measured travel time, resulting from reverberation of waves between the WC anvil and sample, was also corrected at high pressures (~0.5 ns for P wave and ~2.5 ns for S wave).

RESULTS AND DISCUSSION

The travel times for both P and S waves show monotonic decrease with increasing pressure to P >12 GPa, amounting to ~9% and ~6%, respectively (Fig. 1 and Table 1). The measurements from two P-wave experiments are reproducible within 0.5 ns which is approximately the uncertainty of the current measurements. The discrepancy in these two experiments reflects primarily the uncertainty in the pressure measurements. From the travel times of P and S waves and their zero pressure values, the sample lengths and densities at elevated pressures were calculated using the method of Cook (1957), from which P and S wave velocities as well as the elastic longitudinal ($L = \rho V_p^2$) and shear ($G = \rho V_s^2$) moduli were subsequently obtained. The bulk modulus is calculated using the relationship $K = L - 4G/3$. Fitting velocity data to the third order finite strain equations (Davies and Dziewonski 1975) provides simultaneously the elastic moduli at ambient conditions and their pressure derivatives. When calculating the elastic properties, the travel times of both P and S waves at the same pressure are required.

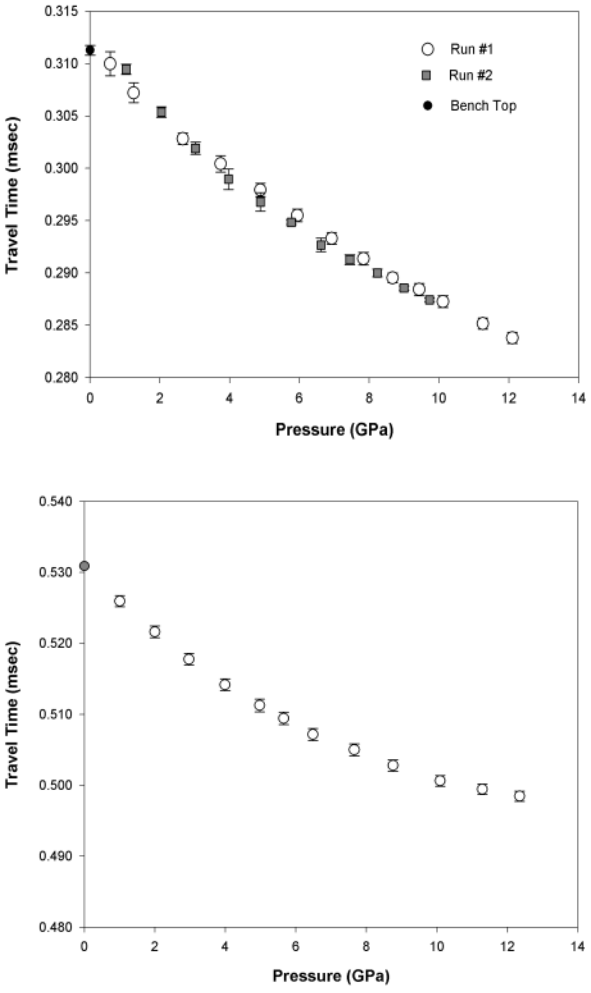

FIGURE 1. (**top**) P wave travel times at high pressure from two experiments. The reproducibility is about 0.5%, which is about the uncertainty of the current measurements. Empty circle and solid square = high pressure run data, solid circle = bench-top results. (**bottom**) S-wave travel times at high pressure. Empty circle = high pressure run data, solid circle = bench-top results.

TABLE 1. Calculated properties of Mg_2SiO_4 spinel from P and S wave experiments*

P (GPa)	$2t_s$ (μs)	ρ (g/cm³)	$2L$ (mm)	V_s (km/s)	G (GPa)
		S wave data			
0.0	0.5308	3.515	3.070	5.78	117
1.0	0.5260	3.534	3.065	5.83	120
2.0	0.5216	3.553	3.059	5.86	122
3.0	0.5178	3.571	3.054	5.90	124
4.0	0.5142	3.590	3.049	5.93	126
5.0	0.5113	3.606	3.044	5.95	128
5.7	0.5094	3.618	3.041	5.97	129
6.5	0.5072	3.633	3.037	5.99	130
7.7	0.5050	3.653	3.031	6.00	132
8.8	0.5028	3.671	3.026	6.02	133
10.1	0.5006	3.693	3.020	6.03	134
11.3	0.4995	3.712	3.015	6.03	135
12.3	0.4985	3.729	3.010	6.04	136
		P wave data			
P (GPa)	$2t_p$ (μs)	ρ (g/cm³)	$2L$ (mm)	V_p (km/s)	L (GPa)
0.0	0.3113	3.515	3.070	9.86	343
1.2	0.3072	3.539	3.063	9.97	352
2.7	0.3028	3.565	3.056	10.09	363
3.7	0.3004	3.584	3.050	10.15	369
4.9	0.2980	3.604	3.044	10.22	376
5.9	0.2955	3.623	3.039	10.28	383
6.9	0.2933	3.640	3.035	10.35	390
7.8	0.2914	3.655	3.030	10.40	395
8.7	0.2895	3.669	3.026	10.45	401
9.4	0.2884	3.682	3.023	10.48	404
10.1	0.2873	3.693	3.020	10.51	408
11.3	0.2852	3.712	3.015	10.57	415
12.1	0.2838	3.725	3.011	10.61	419

* The uncertainty in pressure is about 0.1 GPa. The travel time has a standard deviation less than 0.5 and 1.0 ns for P and S waves, respectively, at the 95% confidence level. The overall uncertainty propagated into the calculated velocity is better than 0.5% while the modulus is about 1%. Data at $P < 1.0$ GPa are not used in data processing due to poor mechanical coupling between the buffer rod and sample.

TABLE 2. Elastic properties of ringwoodite γ-Mg_2SiO_4 at ambient conditions

	1	2	3	4	5	6	7
V_p (km/s)	9.86(3)	9.75–9.77	9.93	9.85(6)	9.86	–	–
V_s (km/s)	5.78(2)	5.82–5.83	5.87	5.82(3)	5.78	–	–
K (GPa)	185(2)	178/184	190	185(3)	184(3)	181.0(3)	182(3)
G (GPa)	120(1)	120/120	125	120(2)	119(2)	124.2(5)	–
K'	4.5(2)	4.69–4.99	4.19	–	–	4.10(2)	4.2(3)
G'	1.5(1)	1.73–1.78	1.12	–	–	1.2(2)	–

1 = This study, ultrasonic results on polycrystal to P>12 GPa.
2 = Rigden et al. (1991), ultrasonic, polycrystal, up to 3 GPa.
3 = Kiefer et al. (1997), pseudopotential calculation.
4 = Jackson et al. (2000), single crystal, Brillouin scattering, ambient.
5 = Weidner et al. (1984), single crystal, Brillouin scattering, ambient.
6 = Matsui (1999), MD simulation.
7 = Meng et al. (1994), static compression, EOS, isothermal values.

Therefore, in processing S-wave data, P-wave travel times at the pressures of the S-wave experiments were obtained from a polynomial fit to the data of Experiment no. 1 (Fig. 1a). The same procedures were performed while processing P-wave data. The results for P- and S-wave experiments conducted at comparable pressure ranges are listed in Table 1.

Finite strain fitting performed on velocity data at high pressures (P > 1.0 GPa) yields K = 185 GPa, G = 120 GPa, K' = 4.5(2), and G' = 1.5(1) for the bulk and shear moduli and their pressure derivatives (Table 2). The elastic moduli at zero pressure are remarkably consistent with previous experimental results of K = 184–185 and G = 119–120 GPa from single-crystal Brillouin scattering measurements (Weidner et al. 1984; Jackson et al. 2000) and the isothermal value of K = 182 GPa of Meng et al. (1994). The bulk modulus falls in the ranges of pseudopotential calculation of Kiefer et al. (1997) and MD calculations of Matsui (1999), while the shear modulus is ~4% lower than that predicted in the previous studies.

The pressure derivatives, as seen in Table 2, differ as much as 20% from the results of Meng et al. (1994) obtained at P > 20 GPa and those of Rigden et al. (1991) at 3 GPa. The results from this study obtained at P > 12 GPa fall in between these two previous studies. Further examination of Figure 2 indicated that the bulk and shear moduli from this study in the range of 0–3 GPa agree well with the previous results of Rigden et al. (1991) obtained from ultrasonic velocity measurements on polycrystalline samples to 3 GPa. However, the current data deviate from Rigden et al. (1991) at about 4–5 GPa and fall in between the finite strain extrapolations of Rigden et al. (1991), the finite strain calculations using a combination of zero pressure values from Brillouin scattering and pressure derivatives from Meng et al. (1994) (P > 20 GPa, K' = 4.2), and theoretical calculations of Kiefer et al. (1997) and Matsui (1999).

Comparison of the current results of iron-free ringwoodite with recent data for [γ-$(Mg_{.91}Fe_{.09})_2SiO_4$] from Sinogeikin et al. (2001) [K = 188(3) GPa, K' = 4.1, G = 120 (2) GPa, G' = 1.3(2), Brillouin scattering to 16 GPa] suggests that 9% iron substitution for magnesium in ringwoodite has insignificant effect (<2%) on the elastic moduli but the pressure derivatives are lowered by ~9%. Further examination of the data from Rigden et al. (1991), Sinogeikin et al. (2001), and this study indicates that the apparent discrepancy in pressure derivatives is primarily due to pressure ranges of the experiments rather than the effects of iron. As discussed above, at pressures less than 3 GPa, the bulk and shear moduli data from this study agree well with those of Rigden et al. (1991). It is also evident that the P- and S-velocity data in this pressure range in Sinogeikin et al. (2001) have similar pressure dependences to those of Rigden et al. (1991) (see Fig. 2 of Sinogeikin et al. 2001). Similarly, at pressures between 4 to 13 GPa (despite large scatter in the Brillouin data), the velocities (also elasticity) on 9% iron ringwoodite show good agreement with those observed in our current study (Fig. 2). This agreement suggests that 9% iron plays an insignificant role on the pressure derivatives of ringwoodite in this pressure range. Ignoring the pressure range of these results, one could mistakenly attribute the apparent difference in pressure derivatives to the effect of iron, the use of polycrystalline samples, or systematic differences inherent in the experimental techniques.

WADSLEYITE TO RINGWOODITE PHASE TRANSITION AND THE 520 KM DISCONTINUITY

The property changes associated with the wadsleyite to ringwoodite phase transition was investigated by calculating the compressional and shear wave velocities for wadsleyite and ringwoodite to high pressures at room temperature (Fig. 3). In order to minimize uncertainty in the estimation of the property changes at the transition pressure, pressure derivatives of bulk and shear moduli from previous ultrasonic measurements of

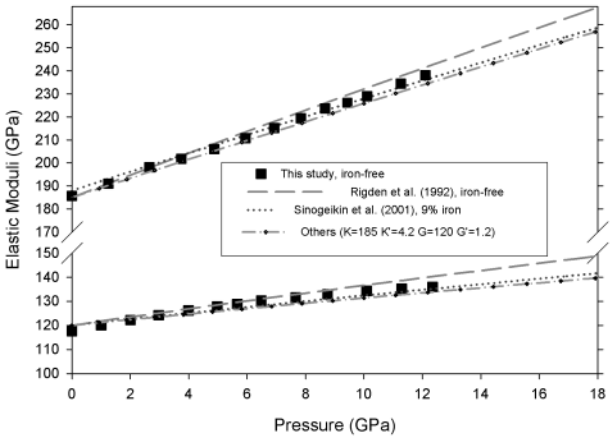

FIGURE 2. Comparison of the bulk and shear moduli at high pressure from this study (filled squares) for iron-free ringwoodite with previous measurements. Long dashed lines are extrapolations of measurements to 3 GPa on iron-free ringwoodite by Rigden et al. (1991), short dashed lines are finite strain calculations using zero pressure values of Jackson et al. (2000) and pressure derivatives from theoretical calculations. Dotted lines are finite strain representation of data from Sinogeikin et al. (2001) for 9% iron ringwoodite.

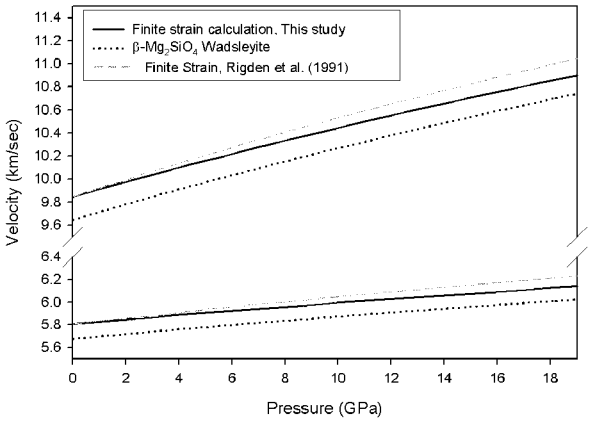

FIGURE 3. Compressional and shear wave velocities of ringwoodite and wadsleyite to 18 GPa. Solid lines: finite strain extrapolation of this study. Dotted lines: Finite strain extrapolations using previous experimental data of Li et al. (1998a) and Zha et al. (1998). Dashed Lines: Finite strain extrapolations of Rigden et al. (1991).

wadsleyite using the same technique over a comparable pressure range were used (Li et al. 1996b). Note that the velocities for ringwoodite and wadsleyite exhibit similar pressure dependence to the pressure at 520 km depth. The velocity difference between these two phases [$V(\gamma)$-$V(\beta)$] amounts to 0.17 km/s and 0.11 km/s at 18 GPa in comparison to 0.21 km/s and 0.14 km/s for P and S waves at ambient conditions. The velocity jumps from wadsleyite to ringwoodite at 520 km pressure (~18 GPa) are ΔV_p = 1.6% and ΔV_s = 1.8% along with a density increase of 2.0%. The resulting acoustic impedance jumps are 3.6% and 3.8% for P wave and S wave, respectively.

When compared with seismic observations, non-olivine components have to be taken into account. It has been shown that interactions among mantle phases through element partitioning have significant effects on the property changes in olivine components throughout the transition zone (Bina and Wood 1987; Irifune and Isshiki 1998; Stixrude 1997; Weidner and Wang 2000). In this study, we investigated the property changes associated with the wadsleyite to ringwoodite phase transition by calculating the velocities around 520 km depth for a pyrolite mantle. Elasticity and iron partitioning among co-existing mantle phases at high pressure and temperature were obtained from extant experimental data (Akaogi and Akimoto 1979; details of the calculation can be found in Weidner and Wang 2000 and Li et al. 2001, and references therein). Elasticity data for ringwoodite used by Weidner and Wang (2000) (see also Duffy and Anderson 1989) were updated with current data for pressure dependence and those from Jackson et al. (2000) for temperature dependence of bulk and shear moduli. The effect of iron on the bulk and shear moduli as well as density was corrected when considering composition changes with increasing depth (e.g., Duffy and Anderson 1989). Although recent experiments have indicated that small amounts of water in wadsleyite and ringwoodite (2 to 3%) cause significant (>10%) decrease of elastic modulus at ambient conditions (Yusa and Inoue 1997; Yusa et al. 2000; Inoue et al. 1998), the amount of water content in the transition zone as well as elasticity data for hydrous wadsleyite and ringwoodite at high pressure and high temperature are still under investigation. The calculations performed here are for an anhydrous mantle composition.

We calculated the velocities for a 1400 °C adiabatic temperature. For a pyrolitic mantle composition, the velocity increase across the wadsleyite to ringwoodite phase transition is 0.4% for P waves, 1.0% for S waves, and 2.1% for density over ~20 km width (Table 3). The resulting acoustic impedance jumps are 2.4% and 3% for P and S waves, respectively. These results are consistent with previous predictions by Rigden et al. (1991) and Weidner et al. (1984) that the dominant feature of the 520 km discontinuity in a pyrolite mantle is a density, rather than velocity, increase. The results of impedance jumps are consistent with the seismic observation of S-wave impedance change of 2.2–3.6% from the SS precursor study of Shearer (1996) and 2.8–4.0% from the ScS reverberation study of Revenaugh and Jordan (1991) near 520 km depth.

Due to the positive Clapeyron slope of the wadsleyite to ringwoodite phase transition (e.g., Katsura and Ito 1989; Morishima et al. 1994), temperature changes cause changes in phase transition pressure and the width of the binary loop, and therefore velocities, impedance, and the width of the phase transition (Bina and Wood 1987). To investigate the effect of temperature on the magnitude and topology of the 520 km discontinuity, velocities around 520 km depth for the pyrolite model along 1200 °C and 1600 °C adiabats were also calculated. The results are summarized in Table 3. At 1200 °C, the wadsleyite to ringwoodite phase transition depth is centered around 500 km, spreading about 30 km in width with total impedance increases of 3.6% and 3.5% for P and S waves, and 2.3% increase in density. In comparison, at 1600 °C, the phase transition width decreases to ~18 km, centered at 552 km, and the impedance increase is 2.3% for P waves, 3.2% for S waves, and 2.2% for density increase. Note that the P-wave velocity

TABLE 3. Comparison of velocity increase, impedance jump and density jump of wadsleyite to ringwoodite phase transition in a pyrolite mantle composition

Adiabat	1200 °C	1400 °C	1600 °C
Depth (km)	484–514	517–537	543–561
ΔV_p (%)	1.3	0.4	0.1
ΔV_s (%)	1.2	1.0	1.0
$\Delta\rho$ (%)	2.3	2.1	2.2
$\Delta(\rho V_p)$ (%)	3.6	2.4	2.3
$\Delta(\rho V_s)$ (%)	3.5	3.1	3.2

jump decreases rapidly with increasing temperature, but S-wave velocity and density jumps remain relatively insensitive to temperature. Similarly, S-wave impedance shows less sensitivity to the variation of temperature than P-wave impedance at this temperature range. These results suggest that cooler temperatures make the 520 km discontinuity less visible than in hot regions mainly by broadening the widths of the discontinuity and decreasing the effective reflection coefficient. This will explain in part the difference in ocean-shield difference in the occurrence of the 520 km discontinuity (Gu et al. 1998). Interestingly, if we consider temperature only, the depth variation of the 520 km discontinuity (484–543 km) in the temperature range of 1200–1600 °C agrees very well with the magnitude of this discontinuity obtained by Flanagan and Shearer (1998) (490–537 km). However, the splitting of the 520 km discontinuity observed by Deuss and Woodhouse (2001) is not obvious in our calculated velocity profiles.

In summary, the available experimental data indicate that the wadsleyite to ringwoodite phase transformation in a pyrolite composition would be visible in seismic data primarily as a density jump over a depth of ~20 km. The results of the impedance jump (3.1–3.5% for S waves, 2.3–3.6% for P waves) and depth (484 to 543 km) for the wadsleyite to ringwoodite transition agree well with the seismically observed 520 km discontinuity at various locations (e.g., Shearer 1996; Revenaugh and Jordan 1991; Ryberg et al. 1997; Deuss and Woodhouse 2001). Lateral temperature variations of ± 200 °C have insignificant effect on the property change of density, S-wave velocity, and S-wave impedance while the depth changes from 484 km to 543 km. Large temperature variations, if they exist in the mantle, could be an alternative to chemical heterogeneity in explaining the large amplitude topography of the 520 km discontinuity.

ACKNOWLEDGMENTS

The high-pressure experiments were performed in the Stony Brook High Pressure Laboratory, which is jointly supported by the State University of New York at Stony Brook and the NSF Science and Technology Center for High Pressure Research (EAR89-20239). This research was partially supported by NSF grants to RCL (EAR93-04502 and 96-14612). The author would like to thank I. Jackson and an anonymous reviewer who helped to improve the manuscript. This is MPI publication No. 308.

REFERENCES CITED

Akaogi, M. and Akimoto, S. (1979) High pressure phase equilibrium in garnet lherzolite, with special reference to Mg^{2+}-Fe^{2+} partitioning among constituent minerals. Physics of the Earth and Planetary Interiors, 19, 31–51.

Benz, H.M. and Vidale, J.E. (1993) Sharpness of upper-mantle discontinuities determined from high- frequency reflections. Nature, 365, 147–150.

Bina, C.R. and Wood, B.J. (1987) Olivine-spinel transitions: experimental and thermodynamic constraints for the nature of the 400 km seismic discontinuity. Journal of Geophysical Research, 92, 4853–4866.

Bock, G. (1994) Synthetic seismogram images of upper mantle structure: No evidence for a 520-km discontinuity. Journal of Geophysical Research, 99, 15843–15851.

Cook, R.K. (1957) Variation of elastic constants and static strains with hydrostatic pressure: A method for calculation from ultrasonic measurements. Journal of the Acoustical Society of America, 29, 445–449.

Cummins, P.R., Kennett, B.L.N., Bowman, J.R., and Bostock, M.G. (1992) The 520-km discontinuity. Bulletin of the Seismological Society of America, 82, 323–336.

Davies, G.F. and Dziewonski, A.M. (1975) Homogeneity and constitution of the Earth's lower mantle and outer core. Physics of Earth Planetary Interior, 10, 336–343.

Deuss, A. and Woodhouse, J. (2001) Seismic observations of splitting of the mid-transition zone discontinuity in Earth's mantle. Science, 294, 354–357.

Duffy, T.S. and Anderson, D.L. (1989) Seismic Velocities in mantle minerals and the mineralogy of the upper mantle. Journal of Geophysical Research, 94, 1895–1921.

Flanagan, M.P. and Shearer, P.M. (1998) Global mapping of topography on transition zone velocity discontinuities by stacking SS precursors. Journal of Geophysical Research: Solid Earth, 103, 2673–2692.

Gu, Y., Dziewonski, A.M., and Agee, C.B. (1998) Global de-correlation of the topography of transition zone discontinuities. Earth and Planetary Science Letters, 157, 57–67.

Inoue, T., Weidner, D.J., Northrup, P.A., and Parise, J.B. (1998) Elastic properties of hydrous ringwoodite (gamma-phase) in Mg_2SiO_4. Earth and Planetary Science Letters, 160, 107–113.

Irifune, T. and Isshiki, M. (1998) Iron partitioning in a pyrolite mantle and the nature of the 410-km seismic discontinuity. Nature, 392, 702–705.

Jackson, J.M., Sinogeikin, S.V., and Bass, J.D. (2000), Sound velocities and elastic properties of gamma-Mg_2SiO_4 to 873 K by Brillouin spectroscopy. American Mineralogist, 85, 296–303.

Katsura, T. and Ito, E. (1989) The system Mg_2SiO_4-Fe_2SiO_4 at high pressures and temperatures: precise determination of stabilities of olivine, modified spinel and spinel. Journal of Geophysical Research, 94, 15663–15670.

Kiefer, B., Stixrude, L., and Wentzcovitch, R.M. (1997) Calculated elastic constants and anisotropy of Mg_2SiO_4 spinel at high pressure. Geophysical Research Letters, 24, 2841–2844.

Li, B., Jackson, I., Gasparik, T., and Liebermann, R.C. (1996a) Elastic wave velocity measurement in multi-anvil apparatus to 10 GPa using ultrasonic interferometry. Physics of the Earth and Planetary Interiors, 98, 79–91.

Li, B., Gwanmesia, G.D., and Liebermann, R.C. (1996b) Sound velocities of olivine and beta polymorphs of Mg_2SiO_4 at Earth's transition zone pressures. Geophysical Research Letters, 23, 2259–2262.

Li, B., Liebermann, R.C., and Weidner, D.J. (1998a) Elastic moduli of Wadsleyite (β-Mg_2SiO_4) to 7 gigapascal and 873 kelvin. Science, 281, 675–677.

Li, B., Chen, G., Gwanmesia, G.D., and Liebermann, R.C. (1998b) Sound velocity measurements at mantle transition conditions of pressure and temperature using ultrasonic interferometry in a multianvil apparatus. In M. Manghnani and T. Yagi, Eds. Properties of Earth and Planetary Materials at High Pressure and Temeprature, p. 41–61. American Geophysical Union, Washington, D.C.

Li, B., Liebermann, R.C., and Weidner, D.J. (2001) P-V-Vp-Vs-T measurements on wadsleyite to 7 GPa and 873 K: Implications for the 410-km seismic discontinuity. Journal of Geophysical Research, 106, 30575–30591.

Liebermann, R.C. and Wang, Y. (1992) Characterization of sample environment in a uniaxial split-sphere apparatus. In Y. Syono and M. Manghnani, Eds., High Pressure Research: Application to Earth and Planetary Sciences, p. 19–31. Terra Scientific Publishing Co., and American Geophysical Union, Tokyo and Washington, D.C.

Matsui, M. (1999) Computer simulation of the Mg_2SiO_4 phase with application to the 410-km seismic discontinuity. Physics of the Earth and Planetary Interiors, 116, 9–18.

Meng, Y., Fei, Y., Weidner, D.J., Gwanmesia, G.D., and Hu, J. (1994) Hydrostatic compression of γ-Mg_2SiO_4 to mantle pressures and 700K: thermal equation of state and related thermoelastic properties. Physics and Chemistry of Minerals, 21, 407–412.

Morishima, H., Kato, T., Suto, M., Ohtani, E., Urakawa, S., Utsumi, W., Shimomura, O., and Kikegawa, T. (1994) The phase boundary between α- and β-Mg_2SiO_4 determined by in-situ X-ray observation. Science, 265, 1202–1203.

Niesler, H. and Jackson, I. (1989), Pressure derivatives of elastic wave velocities from ultrasonic interferometric measurements on jacketed polycrystals. Journal of the Acoustical Society of America, 86, 1573–1585.

Revenaugh, J. and Jordan, T.H. (1991), Mantle layering from ScS reverberations. 2. The transition zone. Journal of Geophysical Research, 96, 19763–19780.

Rigden, S.M., Gwanmesia, G.D., Gerald, J.D.F., Jackson, I., and Liebermann, R.C. (1991) Spinel elasticity and seismic structure of the transition zone of the mantle. Nature, 354, 143–145.

Ringwood, A.E. (1975) Composition and petrology of the Earth's mantle, McGraw-Hill, New York, 618 p.

Ryberg, T., Wenzel, F., Egorkin, A.V., and Solodilov, L. (1997) Short-period observation of the 520 km discontinuity in northern Eurasia. Journal of Geophysical Research, 102, 5413–5422.

Shearer, P.M. (1990) Seismic imaging of upper-mantle structure with new evidence

for a 520-km discontinuity. Nature, 344, 121–126.
Shearer, P.M. (1991) Constraints on upper mantle discontinuities from observations of long-period reflected and converted phases. Journal of Geophysical Research, 96, 18147–18182.
Shearer, P.M. (1996) Transition zone velocity gradients and the 520-km discontinuity. Journal of Geophysical Research, 101, 3053–3066.
Sinogeikin, S.V., Bass, J.D., and Katsura, T. (2001) Single-crystal elasticity of gamma-$(Mg_{0.91}Fe_{0.09})_2SiO_4$ to high pressures and high temperatures. Geophysical Research Letters, 28, 4335–4338.
Stixrude, L. (1997) Structure and sharpness of phase transitions and mantle discontinuities. Journal of Geophysical Research, 102, 14835–14852.
Weidner, D.J. and Wang, Y.B. (2000) Phase transformation: Implication for mantle structure. In S. Karato, A.M. Forte, R.C. Liebermann, G. Masters, and L. Stixrude, Eds., Earth's Deep Interior: Mineral Physics and Tomography From the Atomic to the Global Scale, 117, p. 215–235. Geophysical Monograph, American Geophysical Union, Washington, D.C.
Weidner, D.J., Sawamoto, H., and Sasaki, S. (1984) Single-crystal elastic properties of the spinel phase of Mg_2SiO_4. Journal of Geophysical Research, 89, 7852–7860.
Yusa, H. and Inoue, T. (1997) Compressibility of hydrous wadsleyite (beta-phase) in Mg_2SiO_4 by high pressure X-ray diffraction. Geophysical Research Letters, 24, 1831–1834.
Yusa, H., Inoue, T., and Ohishi, Y. (2000) Isothermal compressibility of hydrous ringwoodite and its relation to the mantle discontinuities. Geophysical Research Letters, 27, 413–416.
Zha, C.-S., Duffy, T.S., Downs, R.T., Mao, H.-K., Hemley, R. J., and Weidner, D.J. (1998) Single-crystal elasticity of the α and β of Mg_2SiO_4 polymorphs at high pressure. In M.H. Manghnani and T. Yagi, Eds., Properties of Earth and Planetary Materials at High Pressure and Temperature, p. 9–16. American Geophysical Union, Washington, D.C.

MANUSCRIPT RECEIVED APRIL 22, 22002
MANUSCRIPT ACCEPTED MARCH 24, 2003
MANUSCRIPT HANDLED BY DONALD ISAAK